Properties of calcium aluminate blended cement incorporating iron-rich slag: Evolution over a curing period of 1 year

Jennifer Astoveza, Romain Trauchessec, Ratana Soth, Yiannis Pontikes

Version of Record: https://www.sciencedirect.com/science/article/pii/S0950061821003299
Manuscript_21c0b75c7760caf078d01c2449bd744d

Properties of Calcium Aluminate Blended Cement Incorporating Iron-rich Slag: Evolution over a Curing Period of 1 Year

Jennifer Astoveza[a,b,c], Romain Trauchessec[b], Ratana Soth[a], Yiannis Pontikes[c]

[a] Science and Technology Department, Imerys Technology Centre- Lyon, 38090 Vaulx-Milieu, France
[b] Institut Jean Lamour, UMR CNRS 7198, Université de Lorraine, IUT NB, BP 90137, 54600 Villers-lès-Nancy, France
[c] KU Leuven Department of Materials Engineering, 3001 Leuven, Belgium

jennifer.astoveza@imerys.com, romain.trauchessec@univ-lorraine.fr, ratana.soth@imerys.com, yiannis.pontikes@kuleuven.be

Abstract

With an outlook directed towards circular economy, the valorization of municipal waste streams and industrial residues has recently conveyed a variety of novel industrial by-products to various applications such as supplementary cementitious materials (SCM) in cement blends or as precursors to inorganic polymers. Despite the synergistic benefits on recycling, reducing the cost and the carbon footprint of cements, the use of such non-conventional SCM is often limited to ordinary Portland cement (OPC)-based formulations. This study investigates the properties of a calcium aluminate cement (CAC)-based blend incorporating 30 wt.% of iron (Fe)-rich slag produced at pilot scale from an industrial lead-zinc production. Compressive and flexural strength (EN 196-1 standard mortars), setting time, dimensional stability (Walter+Bai shrinkage measuring test), early hydration reactions (isothermal calorimetry), and phase assemblage evolution (XRD and TGA) were followed from 1 day to 1 year of curing period for both the slag-containing- and a corresponding reference cement formulation. Additionally, a fast non-destructive technique for quantifying the degree of slag hydration is demonstrated using a combination of X-ray computed tomography (XCT) and volume analysis based on grayscale threshold segmentation. The results from the different techniques suggest the long term (>28 days) reactivity of the slag with the slag-containing mortar sample attaining a comparable compressive strength at 39 MPa versus 41 MPa of the corresponding reference formulation at 90 days. Likewise, the prominent contribution of the slag to the hydration reactions is manifested by the differences in the evolution of the phase assemblage of the two formulations. The degree of slag hydration was calculated to progressively increase over time reaching up to 49% after 1 year of hydration based on the XCT scans. These results along with the long term dimensional stability of the

slag-containing formulation support the potential for valorization of the Fe-rich slag as SCM in the CAC-based blend.

Keywords

calcium aluminate blended cement, non-ferrous metallurgy slag, SCM, tomography, dimensional stability

1 Introduction

The incorporation of supplementary cementitious materials (SCM) in blended cements has been explored for decades primarily as a sustainable pathway for reducing the carbon footprint of cement, or for reducing the binder cost in construction. Naturally-available pozzolans (i.e. pyroclastic pumices, zeolite tuff) and industrial by-products (i.e. ground granulated blast furnace slag, fly ashes, waste glass) are obvious choices considering their reactivity, abundance, low cost and low carbon footprint allocation [1,2]. However, their limited and often localized availability pose a challenge in meeting the demand in construction application.

In the recent years, the Circular Economy Action Plan (COM/2015/614) introduced by the European Commission has motivated a number innovative pathways directed towards a circular economy [3]. Along with the novel technologies being developed, new streams of by-products are generated as secondary resources for the extraction of valuable components and critical elements while leaving metal-extracted residual streams available for further valorization. This has driven interests to their potential use as non-conventional SCM in cement blends while subsequently attempting to address the impending shortage of the conventional products [4]. However, as these new materials originate from varying municipal and industrial process streams, they could be highly heterogeneous, contain hazardous components, and have low inherent hydraulic and pozzolanic potential when compared to the more traditional SCM; therefore requiring pre-treatment ranging from mechanical (i.e. grinding, pre-sorting, sieving), chemical (i.e. aging, leaching) to thermal processing [2,5,6]. A screening test to assess the reactivity of non-conventional SCM (raw non-ferrous metallurgy slags, fumed fayalite slag and municipal waste incinerator bottom ash) in a calcium aluminate cement-based (CAC) formulated binder system has been presented in a preceding study [7]. The results suggested that among the by-

products investigated, the highly amorphous Fe-rich non-ferrous metallurgy slag could have the highest potential as SCM in the CAC dry mix mortar system displaying a long term reactivity indicated by its compressive strength evolution.

Balancing the highly amorphous component of non-ferrous metallurgy slags is a minor crystalline fraction largely dominated by fayalite (Fe_2SiO_4), olivine and spinel group phases [8]. These slags often contain trace elements (As, Cd, Co, Cu, Cr, Mn, Ni, Pb, and Zn) raising concerns on their heavy elements' and toxic components' leachability [8,9]. Nonetheless, their pozzolanic potential has been widely demonstrated in previous studies [10–12] which could be further improved through various activation techniques such as granulation to obtain maximal amorphous fraction and finer milling to increase the exposed surface area [13,14]. Furthermore, their high specific gravity and their particles' sharp angularity have been previously associated to stability, soundness and abrasion resistance in concrete applications [9]. Despite the seemingly limited studies exploring the utilization of similar non-ferrous metallurgy slags in construction applications, promising performance has been reported in terms of the strength, durability and toxicity of the blended formulations [8,9,13,15–19]. However, these studies were mostly limited to applications in OPC-based systems as substitute to aggregates in concrete and as Fe source in the raw meal, primarily because a significant decrease in reactivity has been demonstrated when used as SCM at higher replacement levels (>40 wt.%) [9].

The use of non-ferrous metallurgy slags as SCM in CAC-based binder formulation is a novel approach which has not been investigated previously. There is a substantial gap to be filled in understanding the hydration mechanism of Fe-rich non-ferrous metallurgy slags in the system given the limited thermodynamic data, hindering predictions as to the hydrate phase/s formed when the Fe from the slag is dissolved. In pure CAC systems with monocalcium aluminate (CA)[1] as the main anhydrous phase, the hydration initially results in the formation of metastable calcium aluminate hydrate phases (CAH_{10}, C_2AH_8, AH_3) when cured below 27°C, which at long term or at high temperature curing transform into stable hydrogarnet (C_3AH_6) − a reaction called "conversion". Since C_3AH_6 has higher density than the metastable hydrate phases, conversion is known to cause a subsequent decrease in strength resulting from the volume change and therefore a higher susceptibility to failure [20]. To avoid this

[1] Cement shorthand notation : C: CaO, A: Al_2O_3, $: SO_3, S: SiO_2, c: CO_2, F: Fe_3O_4, T: TiO_2, H: H_2O

phenomenon in industrial applications, sulfate source is added to CAC-based formulations not only to retard the setting time but also to favor the formation of Al_2O_3–Fe_2O_3-mono and -tri phases (AFm and AFt respectively) over that of the metastable calcium aluminate hydrates. Such sulfated CAC systems are primarily dominated either by ettringite ($C_3A•3C\$•H_{32}$), monosulfoaluminate ($C_3A•C\$•H_{12}$), or with the addition of SCM as a silicate source, by strätlingite (C_2ASH_8) – three hydrate products noted to contribute to the strength development of hardened blends [21–23].

In this paper, the properties of a ternary binder consisting of CAC, calcium sulfate hemihydrate (HH) and an Fe-rich non-ferrous metallurgy slag (slag) is investigated during curing for one year. The early-age reactivity of the slag was characterized in paste samples using isothermal calorimetry. The compressive and flexural strength (EN 196-1 standard mortars), setting time, dimensional stability (Walter+Bai shrinkage measuring test), and phase assemblage evolution (XRD and TGA) were subsequently followed. Finally, a rapid non-destructive technique to quantify the degree of slag hydration using a combination of X-ray computed tomography (XCT) and image analysis based on the grayscale allocation [24] of the 3D reconstructed models of the ternary blend is presented.

2 Materials and Methods

The slag used in this study is coming from a pilot-scale thermal treatment of an Fe-rich residue originating from a lead-zinc plant. Granulation rendered the glassy structure of the slag leaving only 8 wt.% crystalline phase, wüstite (FeO). Its reactivity is assessed in a formulation mainly consisting of Secar 51, a fused CAC commercial product chosen for its relatively low iron content. It is composed of >60 wt.% monocalcium aluminate (CA) with the balance predominated by gehlenite (C_2AS), belite (C_2S), perovskite (CT) and spinel ($MgAl_2O_4$). Calcium sulfate β-hemihydrate (HH, Prestia Selecta from Lafarge) was added in the formulation to control the setting time and the phase assemblage during hydration. Millisil E400® (quartz filler) served as an inert substitute to differentiate filler effect from slag reactivity. The chemical composition of the raw materials was measured using semi-quantitative Bruker S4 Pioneer X-ray fluorescence (XRF) using back-loading technique to mitigate preferred orientation. The Micrometrics AccuPyc II 1340 pycnometer system was used to measure their density through helium displacement. Particle size distribution was determined using the

Malvern Mastersizer 3000 laser diffraction system while the specific surface areas presented were measured using a semi-automatic Blaine Air Permeability Apparatus and the Micrometrics BET Tristar 3000 using nitrogen as adsorbate. The D8 Advance X-ray Diffractometer (XRD) from Bruker coupled with LynxEye detetor was used to analyze the mineralogy of the raw materials. It was operated using the CuK_{α} (1.54 Å) radiation, scanning at 2θ range of 5-80°, with a step size of 0.02° and a counting time of 1.84 seconds per step. Phase identification and quantification were done on the software DiffracEVA v3 and TOPAS v3 respectively. To quantify the amorphous content of the raw slag, Rietveld analysis was performed on the slag sample adding 10 wt.% of analytical grade ZnO as an internal standard.

The powder diffractogram of the raw materials and a summary of their properties are presented in **Figure 1** and **Table 1** respectively. The particle size distribution and the Blaine specific surface area of the slag obtained after milling in a laboratory ball mill is presented in **Table 2** and considered to be comparable to those of the CAC and the quartz filler used in this study.

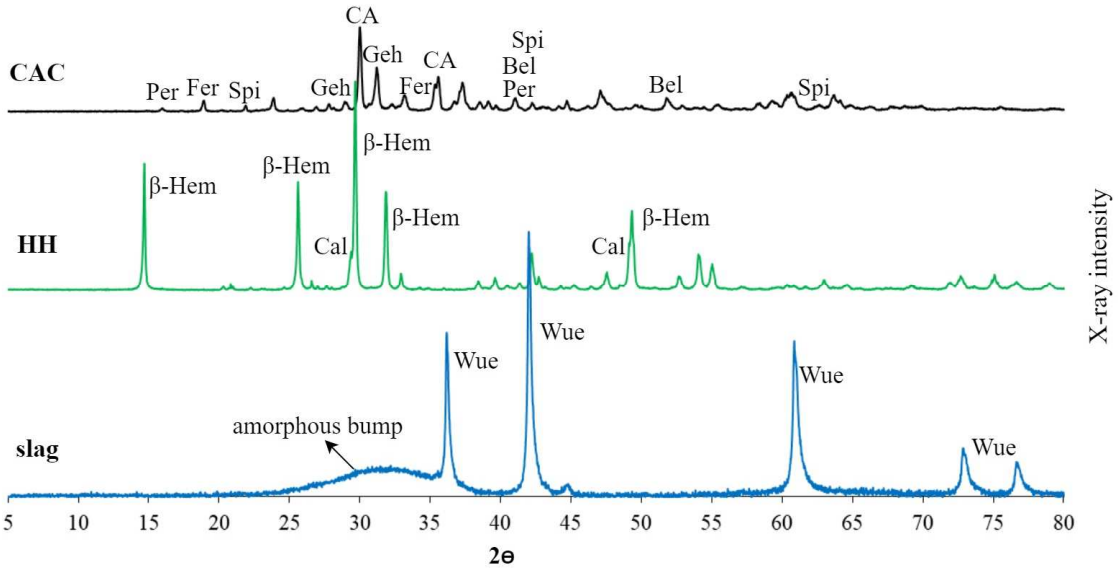

Figure 1 XRD patterns of the raw materials following the abbreviations: perovskite (Per), ferrite (Fer), spinel (Spi), gehlenite (Geh), monocalcium aluminate (CA), belite (Bel), beta-hemihydrate (β-Hem), calcite (Cal), wüstite (Wue)

Table 1 Chemical analysis and density of the raw materials used. The symbol " – " indicates that no measurement was made due to the expected negligible value in case present, while "<dl" indicates that the value is below the lower detection limit of the device (0.0001 %)

	CAC	quartz filler	slag	HH
Density, g/cm^3	3.02	2.66	3.67	2.64
Amorphous content, wt.%	–	–	92	–
Chemical composition, wt.%				
CaO	37.7	<dl	13.6	41.7
Al_2O_3	52.3	<dl	5.2	0.1
SiO_2	4.9	99.8	28.1	0.8
Fe_2O_3 (CAC, HH); FeO (slag)	1.8	<dl	41.4	0.1
MgO	0.4	<dl	2.4	0.1
SO_3	0.2	<dl	0.8	56.5
K_2O	<dl	<dl	0.7	<dl
P_2O_5	0.1	<dl	0.2	<dl
Na_2O	<dl	<dl	4.3	<dl
Cr_2O_3	0.1	<dl	0.1	<dl
CuO	<dl	<dl	0.4	<dl
ZnO	<dl	<dl	<dl	<dl
Others	2.5	0.2	2.8	0.7

Table 2 Particle size distribution and specific surface area of the raw materials used in preparing the dry mix

	Particle Size Distribution (µm)			Specific Surface Area	
	d10	d50	d90	Blaine (cm^2/g)	BET(m^2/g)
slag	1.1	7.9	50.5	4370	1.352
CAC	1.1	11.6	52.3	4270	1.019
quartz filler	1.2	12.4	40.6	4580	1.118

Standard mortars were prepared with a constant CAC to HH mass ratio of 4.5 and a water to binder ratio (w/b) of 0.5 following the formulation shown in **Table 3**. The slag-containing formulation (CAC-HH-slag) was derived by replacing 30 wt.% of the binder (CAC and HH) of the reference cement formulation (CAC-HH) by the slag, while the filler-containing formulation (CAC-HH-quartz) was derived by replacing the slag in the CAC-HH-slag formulation by the same volume of the inert quartz filler. Compressive and flexural strengths were determined according to the EN 196-1 standard followed by curing under water at 20°C after demoulding at 1 day. Strength activity index (SAI) was calculated by dividing the compressive strength of the mortars containing SCM (CAC-HH-quartz or CAC-HH-slag) over that of the reference cement formulation (CAC-HH). Initial and final setting times were measured at 20°C with a portion of the freshly mixed blend for mortars as samples, using the Vicatronic Automatic Vicat Machine without submersion in water during the test. Dimensional variations in the first 24 hours of hydration were measured using the Walter+Bai shrinkage measuring test device type SWG-H-400 on a 70 x 70 x 70 mm^3 (max. length 400 mm) triangular prism mortar samples. The same mortar samples were demoulded after 24 hours and cured under water at 20°C. Dimensional variation throughout the curing time was continuously monitored using an extensometer (0.001 mm precision) with the reference length taken right after the time of demoulding.

Table 3 Mortar formulation (expressed in weight percentage)

		CAC-HH		CAC-HH-quartz		CAC-HH-slag	
binder	CAC	18	22	13	21	13	22
	HH	4		3		3	
	SCM	0		5		7	
water		11		11		11	
sand		67		69		67	

Paste samples were likewise prepared using the same binder formulation as the standard mortars but with a w/b ratio of 0.6 using 100 g of dry mix formulation per batch and a mixing time of 2 min performed at 250 rpm with a laboratory electric agitator directly after the water is added. Ex-situ isothermal calorimetry (TAM Air, TA instruments) was performed on freshly prepared pastes taking 10 g of sample from the bulk paste mixtures to follow the heat release during the first 7 days of hydration at 20°C. The remaining paste mixtures were cured hermetically in sealed plastic bottles at 20°C. At each age (1, 7, 28, 90, 180 and 365 days), the hydration of the pastes was stopped through solvent exchange by immersing the crushed samples in isopropanol for 5 days followed by immersion in diethyl ether to aid the drying. The phase assemblages of the hydrated pastes after stopping the hydration were identified using the same XRD procedure as the raw materials. The samples were likewise subjected to thermogravimetric analysis using the Mettler Toledo TGA/DSC Simultaneous Thermal Analyzer. Since free water is supposed to be removed during the solvent exchange, bound water content was assumed to correspond to the water loss measured between 50-500°C under N_2 atmosphere heated at a rate of 30°C/min.

Moreover, fragments of the standard mortar samples subjected to the solvent exchange for stopping the hydration as previously described but with longer immersion in isopropanol (7 days), were impregnated under vacuum with an epoxy resin (EPOXYPACK 301) and polished with diamond spray ranging from 9 to ¼ µm. The polished sections were examined under SEM (ThermoFischer Quanta 250 FEG) backscattered electrons (BSE) and energy dispersive X-ray analysis (EDS) operated at an accelerating voltage of 20 kV.

Finally, in an attempt to follow and quantify the degree of slag dissolution during hydration, micro-CT image acquisition (Phoenix Nanotom S, GE Inspection Technologies X-ray computed tomography system) was performed on the slag-containing paste formulation. A small fracture of the hardened paste was taken after 24 hours of curing and wrapped entirely with Parafilm without stopping the hydration. Tomographic projections were acquired for a 360° rotation angle, with a 0.15° rotation step, in nanofocus mode 1. X-ray source voltage and current were set at 90 KV and 170 µA respectively for all scans. The installed target material consisted of tungsten on CVD synthetic diamond. A 0.1 mm thick copper filter material was installed during the scans to harden the X-ray beam before it reached

the sample. The isotropic voxel resolution in all scans was set to 2.15 µm, specifically chosen to be smaller than most of the slag particles of interest, while still keeping the detector field of view large enough to scan a representative sample volume. With the exposure time set to 500 ms, skip setting to 1, and requesting 2400 projections, a scan time of 1 hour and 26 mins was achieved. Datos|x software was used to reconstruct the micro-CT scans and to export cross-sectional stack images. Grayscale threshold segmentation was performed on the 16-bit reconstructed stack images using the Bruker CT-Analyser (CTAn) v 1.18.8.0+ software followed by conversion to an 8-bit grayscale stack images for further image processing. A standard series of operations pre-programmed in CTAn (Filtering, Thresholding, Despeckle) were performed consistently to all the converted cross sections at all curing ages. 3D volume renderings of the sample matrix and slag particles were generated in Bruker CTVox v 3.3. The same hardened paste sample was analyzed after 1, 28, 90, 180 and 365 days of hydration with the aim of following the total volume covered by the slag at each curing time therefore following the slag dissolution and assuming its direct correlation to the slag reactivity. The slag total volume obtained at day 1 was used as the base value (zero reactivity reference) in calculating the degree of slag reactivity after 28, 90, 180 and 365 days.

The calculated values were compared to a previous experiment which results were included in an oral presentation for a past conference [25]. The same paste formulations, raw materials and curing conditions were used in the earlier study. However, stopping of hydration via solvent exchange was performed prior to the XCT scan and therefore, different samples from the same batch of paste preparation had to be used per scan to represent a curing period (1 day and 90 days). The same voltage and current setting were used for the scans (90 KV, 170 µA) but the isotropic voxel resolution was finer at 1.5 µm. A 0.1 mm thick aluminum filter material was also installed in addition to the copper filter during the scans and the fast scan mode was activated completing the full run only after 20 minutes. After reconstruction using the Datos|x software and selecting a cylindrical VOI (as opposed to a cubic VOI used in the current study), the data was further processed using Matlab (2016) and the 2D/3D image analysis software Avizo (2019.1). In a first step the slag particles (foreground voxels) were separated from the matrix (background voxels). For this step a double threshold hysteresis

function was used, which returns a binary version of the original grayscale image, based on two predefined thresholds (a weak one, Tw and a strong one, Ts). Gray values in the histogram below Tw are labeled as background in the segmented image, while those above Ts are labeled as foreground. Subsequently, gray levels that fall in between Tw and Ts are labeled as matrix or slag particle, depending on their 4-way connectivity to labeled areas in the segmented image. 3D volume renderings of the sample matrix and slag particles were generated in Avizo. To complement the results from XCT, image processing using Image J software was performed for SEM micrographs performed on a portion of the same hydrated paste samples to quantify the slag reaction degree in terms of the changes in the total slag area. Although these latter results (quantification by SEM) are excluded from this paper, it must be noted that this complementary technique was effective not only in verifying the slag volumes calculated from the analysis using XCT but more importantly in accurately identifying the smaller slag particles using the EDS detector.

Finally, a sensitivity analysis was performed in function of the grayscale threshold limit assigned to the slag particles for the samples without the hydration stoppage procedure (solvent exchange) to demonstrate the impact of threshold segmentation to the calculated volume. The degree of slag hydration calculated based on the change of the total slag percent volume for the experiment with samples hydrating continuously, is compared to the calculated values from the earlier experiment using samples after solvent exchange to further assess the sensitivity of the results between the two different methodologies. This comparison aims to challenge the reliability of the XCT and volume analysis in quantifying the degree of slag hydration.

3 Results and Discussion

3.1 Physical properties of mortar formulations and isothermal calorimetry curves

The initial and final setting times of the reference cement formulation (CAC-HH), the reference formulation with the inert quartz filler (CAC-HH-quartz), and the slag-containing formulation (CAC-HH-slag) are presented in **Figure 2**. The results agree with the general trend that most of the SCMs have the tendency to prolong the setting time particularly at lower replacement levels [26]. In the CAC-HH-quartz and CAC-HH-slag formulations, the lower amount of CAC which is known to yield

the “rapid setting and hardening” [21] property of the blend could be regarded as the main factor for the few minutes of retardation in the setting time. It appears that the substitution with the slag caused a modest delay in the initial setting time (1.87 min) and the final setting time (0.94 min) when compared to the reference cement formulation. Although a number of studies with conflicting results depicting either positive or negative deviations from the reference with the slag replacement were cited in Juenger et al [27], the replacement level, slag composition, fineness and the curing conditions are only some of the various factors that could explain the differences among the results of previous studies and this experiment. Moreover, despite the equal volume substitution of the slag with the quartz filler and the comparable PSD and SSA of the raw materials (**Table 2**), it is clear that slag addition can convey effects to the physical properties of the blend different from that of an inert quartz filler.

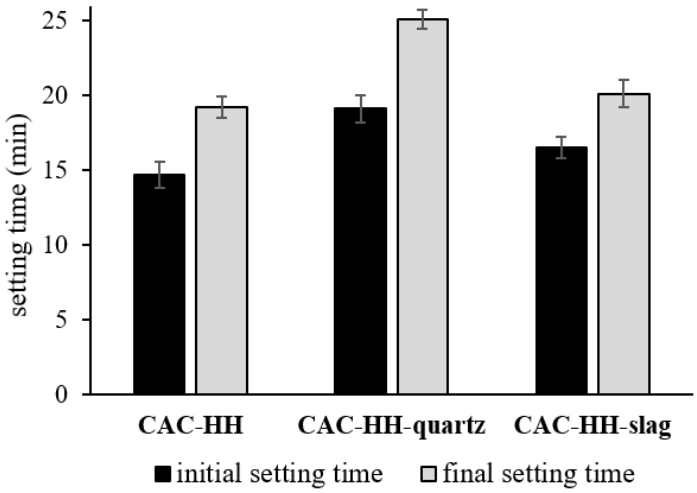

Figure 2 Initial and final setting times of the CAC-HH, CAC-HH-quartz and CAC-HH-slag formulations measured from a portion of the freshly-mixed blend for mortars using the Vicatronic Automatic Vicat Machine at 20°C without submersion in water

The evolution of (a) compressive and (b) flexural strength of the three formulations (CAC-HH, CAC-HH-quartz and CAC-HH-slag) along with the calculated SAI after 1, 7, 28, 90, 180 and 365 days of curing are shown in **Figure 3** below. Unlike the rather comparable flexural strength trend among the three formulations in the early period of hydration, the incorporation of slag clearly resulted in a substantial decrease in the early compressive strength compared to the reference formulation peaking at 31% reduction at day 1. The diminishing trend of the compressive strength was not repressed until

beyond the 28 days curing as the difference in the strength dropped to only 4% versus the reference upon reaching 90 days. The same effect of early compressive strength reduction has been demonstrated for various types of municipal wastes and industrial by-products as presented in a preceding study [7]. This is directly linked to the slower dissolution of the by-products in the solution compared to the cementitious component (CAC and HH) thereby failing to yield a substantial (if any) contribution to the strength and consequently acting only as an inert filler during the early age of hydration. Slower dissolution rate is not only noted for these by-products but is prominent even with most of the traditional SCM [1]. This low early strength could be further associated with the heat release curves shown in **Figure 4**. The addition of the slag in the system lowered the total heat release of the hydrated paste at least in the first 7 days of hydration on a comparable degree obtained with the addition of the inert quartz filler. The mechanism of early age hydration appears to be unaltered with the addition of slag preserving the three main peaks although with a seemingly slower kinetics compared to the reference cement formulation. As already presented in previous studies [7,21], these three main peaks in the ternary blend of CAC, HH and slag represent: the abrupt dissolution of hemihydrate leading to rapid gypsum precipitation (a-b); dissolution of CA and gypsum resulting to massive ettringite precipitation (b-c); and monosulfate formation as gypsum is depleted (c-d).

After 90 days of curing, the compressive strength of the CAC-HH-slag mortars ramped up deviating significantly from that of the CAC-HH-quartz formulation. The evolution of SAI (for compressive strength) clearly indicates the long term reactivity of the slag in the CAC-based formulation significantly surpassing the values of CAC-HH-quartz. From these results, it can already be deduced that it is likely the slag had an effect on the long term hydration reactions due to the dissolution effects occurring over time particularly beyond 28 days.

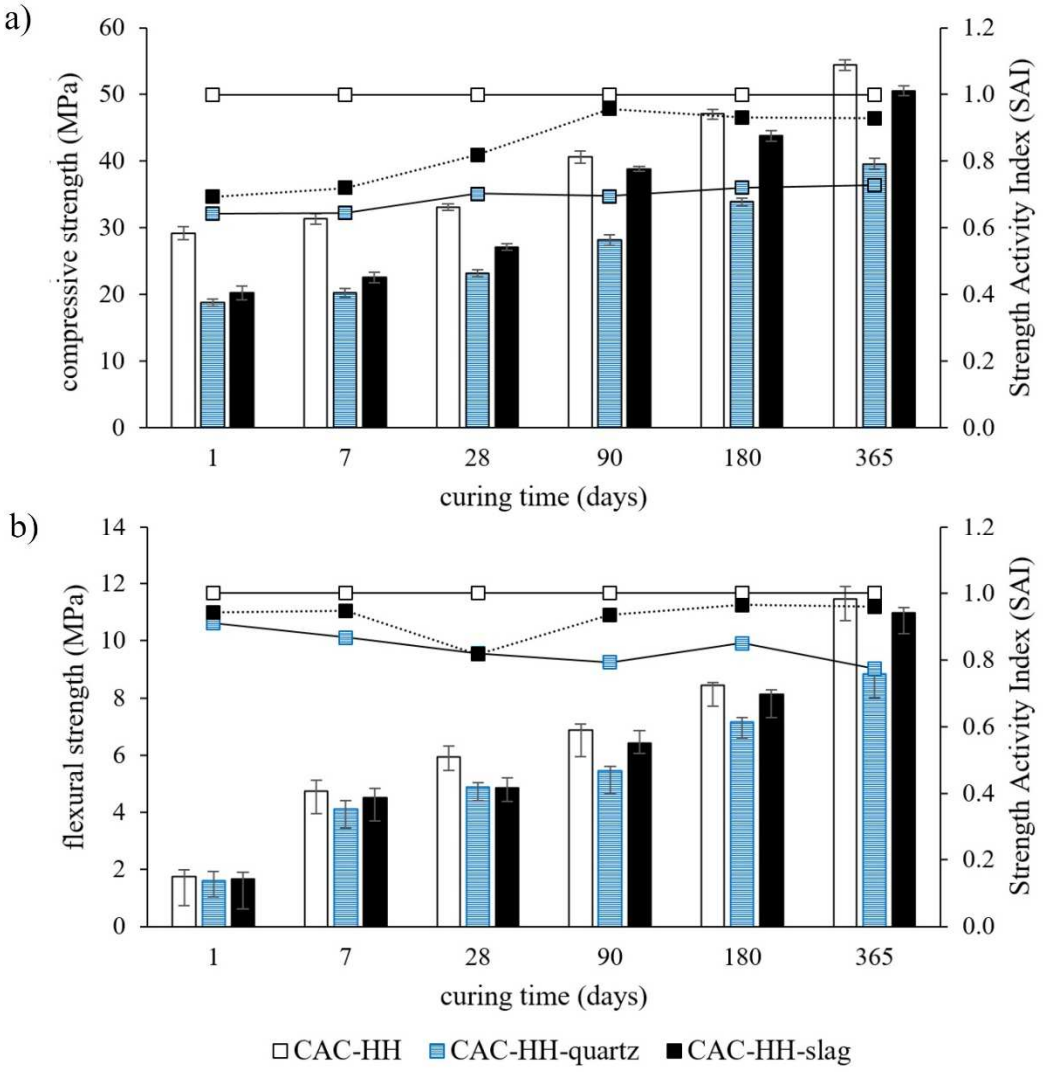

Figure 3 On the primary axis: the evolution over time of the (a) compressive strength and (b) flexural strength of standard mortars with error bars representing the standard deviation among 3 mortar samples. On the secondary axis: the strength activity index (SAI) calculated as the ratio of the(a) compressive/ (b) flexural strength of the quartz filler- (CAC-HH-quartz) or the slag-containing mortar (CAC-HH-slag) to that of the reference cement mortar (CAC-HH)

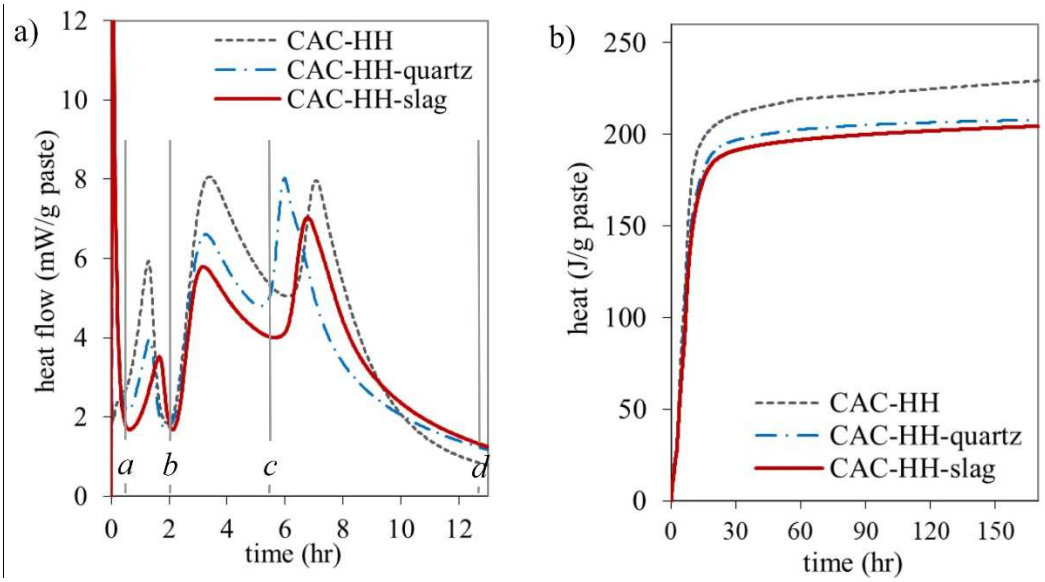

Figure 4 (a) Heat flow and (b) cumulative heat release per gram of paste during the hydration of CAC blended with HH and Fe-rich slag

Despite the lower early compressive strength of the CAC-HH-slag formulation, the interest in the proposed valorization – especially in non-structural applications such as those with the typical finishing operations using CAC [28] – remains rational given the flexural strength evolution in **Figure 3** b. This can be further motivated by the dimensional stability of the formulation demonstrated by the results in **Figure 5**. It can be seen that the incorporation of the slag in the cementitious system had no significant impact to the general trend of dimensional variation compared to the reference formulation. Shrinkage appears to dominate the first day of curing while the expansive nature [29] of ettringite formation could be hypothesized to slightly alter the early hours' trend. Coinciding with the isothermal peak for ettringite precipitation (**Figure 4**) between 2-6 hours, a small expansion peak is present for both formulations just before reaching 6 hours. Between 6 to 18 hours, the reference formulation, CAC-HH, appears to be dimensionally stable possibly resulting from the fast formation of interlocking ettringite crystals balancing out the shrinkage for some hours. On the other hand, a more abrupt shrinkage was noted for CAC-HH-slag after 6 hours which could be an indication of lesser expansive hydrate formation affirmative to the initial indications from the heat release curves. After 24 hours, a slight expansion is observed triggered by the water curing procedure following the demoulding of the samples. This step provides additional free water to the system which could

stimulate hydration while simultaneously avoiding drying shrinkage throughout the remaining duration of curing. From day 1 to 1 year of curing under water, the mortar samples remained dimensionally stable manifesting through the continuous strength development over time in **Figure 3**. In the end it is important to note that despite the seemingly lower effective dimensional stability of the CAC-HH-slag formulation, the scale of the dimensional change comparing the trends is low (difference of ≈ 0.05 mm/m) and could well fall within the confidence interval of the test.

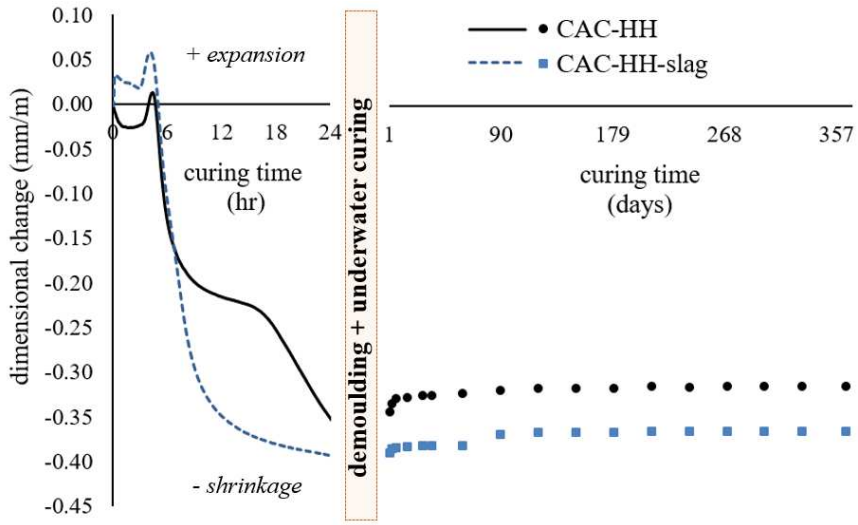

Figure 5 Expansion of CAC-HH and CAC-HH-slag measured using the Walter+Bai shrinkage test for the first 24 hours of hydration and an extensometer for the demoulded samples from Walter+Bai test water-cured from 1 day to 365 days of hydration at 20°C

3.2 Evolution of phase assemblage over time

The evolution of the phase assemblage of the CAC-HH and CAC-HH-slag paste samples were followed from 1 day to 1 year of hydration using XRD and TGA. Results from XRD (**Figure 6**) revealed that the main hydration products for both the formulations include: ettringite (Ett), strätlingite (Str) and monosulfoaluminate (Ms). It is important to note that the formulations under study is a low-sulfated system with a CAC:HH mass ratio of 4.5. With such low amount of sulfates, the kinetically-favored ettringite that has formed in the early age of hydration eventually converts into a monosulfoaluminate [30,31]. Based on the relative intensities of the diffraction peaks, ettringite appears to dominate both systems in the first 7 days of hydration giving early strength properties and validating the initial findings from the heat release curves. In the slag-containing formulation, the

quantity of ettringite appears to gradually decrease over time suggested by the trend of the diffraction patterns whereas monosulfoaluminate proportion increases as the sulfate source is almost fully consumed during the early hydration. Although the diffraction pattern corresponding to the monosulfoaluminate phase is hardly evident due to its poor crystalline nature, the DTG curves (**Figure 7**) suggest its presence along with another amorphous hydrate product, gibbsite (Gib). Unlike that of the slag-containing formulation, the diminishing ettringite content in the reference formulation seem to be halted for the 90-day samples from both XRD and TGA and started to increase until 1 year of hydration as the hydrogarnet peak (Hdg) appears. This ettringite formation between 90 and 180 days of hydration is not common in CAC-HH systems and should be confirmed using quantitative techniques (Rietveld analysis, amorphous content, etc.). The poorly-ordered crystal structure and the possible composition variability of the monosulfoaluminate [32] are only few of the challenges during the characterization of the main hydrate phases. The diffraction patterns alone could not confirm the absolute amount of the phases especially with the significant amorphous fraction constituting the system. Two possibilities could be attributed to the observed "increase" in ettringite diffraction peak for the CAC-HH formulation after 90 days: (1) the tendency of undesired excessive drying of the 90-day-sample either while curing or during characterization; and (2) the formation of hydrogarnet which alters the stability of monosulfoaluminate and ettringite. In the first case, it might well be that the drop of ettringite content in the 90-day sample made it appear that it falsely reformed on later ages. On the other hand, the second case could be reasoned following a paper of Feng et al [32] which demonstrates several factors influencing the stability of AFm phases (i.e. monosulfoaluminate) using thermodynamic modelling based on Gibbs energy minimization. It was presented that the stability region and the composition of the AFm phase are highly sensitive to hydrogarnet solubility particularly in low sulfate concentrations. This could be relevant given that hydrogarnet formation at later ages is only observed for the CAC-HH formulation. A similar study by Damidot et al [33] demonstrated that several AFm phases become metastable in the presence of hydrogarnet and ettringite below 50°C as AFm only stabilizes when hydrogarnet formation is suppressed in the modelling on the basis that its formation is not thermodynamically favored in the early hydration [32]. Furthermore, the reactivity of the slag becoming more apparent from the 90-day-mortar samples could

bring about changes in the composition and pH of the pore solution possibly triggering the different trends in the diffraction patterns between the reference cement and the slag-containing formulation. In the end, the complexity of the systems would require complementary quantitative characterization to unravel the reactions governing the hydration.

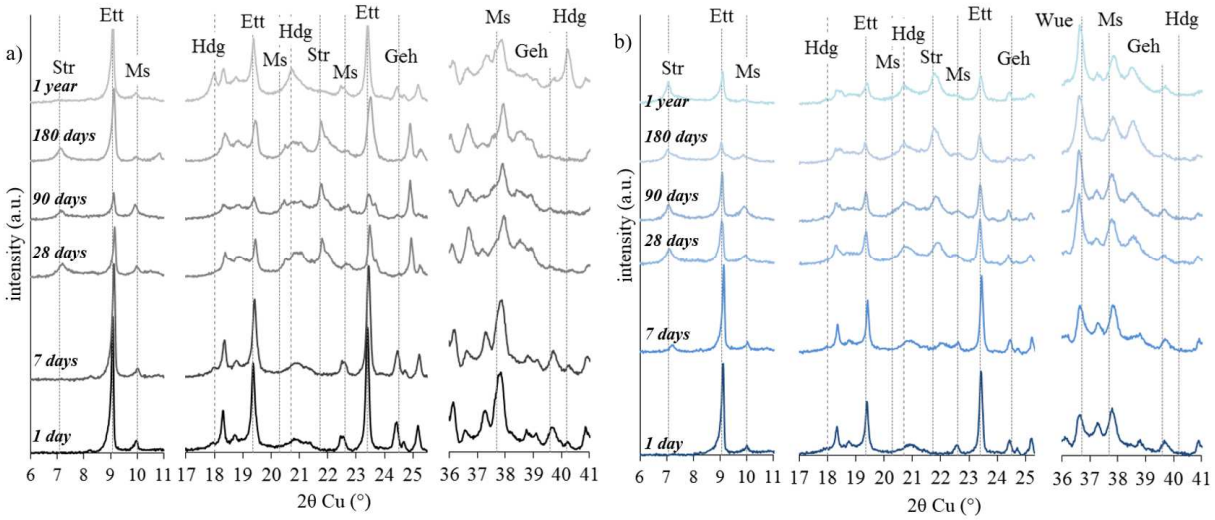

Figure 6 Phase assemblage of the reference, CAC-HH (a), and the slag-containing, CAC-HH-slag (b), paste formulations determined by XRD at 1, 7, 28, 90, 180 and 365 days of curing

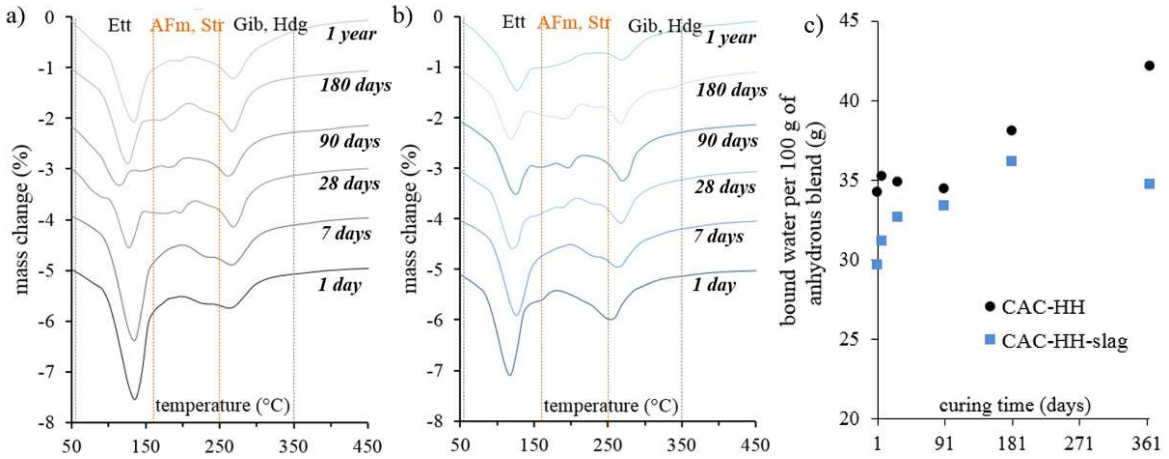

Figure 7 Evolution of the Derivative Thermogravimetric (DTG) curves of the reference, CAC-HH (a); slag-containing, CAC-HH-slag, (b) paste formulations; and (c) the total bound water (50°-500°C) content per 100 g of anhydrous blend determined by TGA at 1, 7, 28, 90, 180 and 365 days of curing

To further discuss the other trends observed from these results, previous studies have reported the benefits of the addition of siliceous pozzolans on the compressive strength of CAC formulations attributed to the formation of denser pore structures [23,34] and to the preferential formation of

strätlingite which inhibits the conversion phenomenon [35–38]. The strength giving property of strätlingite is well-reported in literature [23,39] and is proven superior to that of hydrogarnet [36]. Looking at the phase assemblage of the CAC-HH-slag formulation in **Figure 6**, strätlingite peaks are present from 7 days to 1 year of curing which could be linked to its continuous strength development. On the contrary, the strätlingite peaks occurred later at 28 days for the CAC-HH, disappearing with the formation of hydrogarnet and ettringite for the 1-year sample. It is well-reported in literature [40,41] that the formation AFt phases (i.e. ettringite) suppresses silicates hydration in low-sulfated CAC systems which could be the reason for the observed reduction of strätlingite peaks in the reference cement formulation. Other possible contributions of the slag addition in improving the strength of the CAC blend could be associated to the acidic nature of the slag slowing down the conversion phenomenon [42]; and it may be linked to the increasing SAI trend for the CAC-HH-slag formulation in **Figure 3**.

Furthermore, the seemingly fast consumption of the anhydrous phase gehlenite (Geh), C_2AS, is observed after 7 days in the CAC-HH (**Figure 6**) which is not the case for the CAC-HH-slag formulation probably due to the additional silicates from the slag being consumed either preferentially or along the gehlenite from the CAC. Moreover it is noted that wüstite (Wue), the crystalline component of the slag, appears to be unreactive as its peak remained stable throughout the hydration period. This suggests the preferential dissolution of the amorphous component of the slag over that of the crystalline component in agreement to previous studies on the reactivity of Fe-rich slags [43]. As to the fate of Fe in cement hydration, although existing studies involving synthetic systems suggested incorporation of Fe in the dominant hydrate phases (i.e. ettringite and monosulfoaluminate) as a solid substitute to Al characterized by peak shifts in the diffractograms [44,45], there is no clear indication of such substitution from the results of this study. Likewise, no new Fe-containing hydrate phases were detected from XRD nor TGA alone. In this case, it is likely that Fe is incorporated in amorphous phase/s undetected by XRD and hardly distinguishable in the DTG curves due to possible overlap of decomposition temperatures with the other hydrates. Investigations by Dilnesa et al [45,46] demonstrated that siliceous hydrogarnet is the most stable Fe-incorporating phase in hydrated cements exhibiting a diminishing crystalline structure as iron incorporation increases. From **Figure 7**, it can be

observed that it is indeed difficult to distinguish between the AFm and strätlingite peaks occurring from 160-250°C and between the gibbsite and hydrogarnet peaks from 250-350 °C. In the end, TGA was suitable more for the quantification of the total bound water content as shown in **Figure 7** c. From these results, the increasing bound water content for both formulations is expected as the hydration proceeds and is often associated to the increasing strength of the corresponding mortars. However there is a drastic drop of the bound water content for the CAC-HH-slag formulation for the 1-year-sample which could be associated to the possible conversion of the high bound-water-containing ettringite to monosulfoaluminate. Additionally, Möschner et al [44] noted that the more Fe is incorporated in a hydrate phase, the heavier it becomes and the less water intake it could sustain.

As much remains obscure on the fate of Fe during the slag hydration and in the proportion and stability of the hydrate phases (ettringite, hydrogarnet, etc.) in the long term, further characterization (selective dissolution, Mössbauer spectroscopy, etc.) is recommended in complementary to XRD and TGA. Nonetheless in order to provide more information for these future exploration, it is essential not only to demonstrate the slag reaction but also to quantify the degree of its reactivity. This is addressed in the following section of this study through SEM and XCT.

3.3 Quantifying the degree of slag hydration

The SEM micrograph in conjunction with the BSE detector of the CAC-HH-slag formulation in a mortar sample after 90 days of water-curing is presented in **Figure 8** (a) along with its corresponding EDS maps (b-d). Unlike the CAC particles which start to display dissolution at the surfaces gradually blending into the matrix (formation of hydrate rim), the slag particles appear to be intact with no evidence of hydrate precipitation on their surfaces. Chemical mapping through EDS revealed the massive dispersion of Ca and Al ions throughout the interstices while Fe and Si are mainly localized in the slag and sand particles respectively, validating the much slower reactivity of the slag versus the cementitious components. Moreover with its high Fe content (having higher atomic number), the slag particles appear the brightest in the micrograph compared to the other components (anhydrous CAC, hydrate phases, sand and pores) present. The dendrites of Fe oxides specifically indicative of similar granulated Fe-rich slags as reported by Kero in [43], clearly distinguishes the slag particles from the

other components. These distinctive properties support the viability of quantifying the total area occupied by the slag particles from SEM micrographs through image analysis with high accuracy.

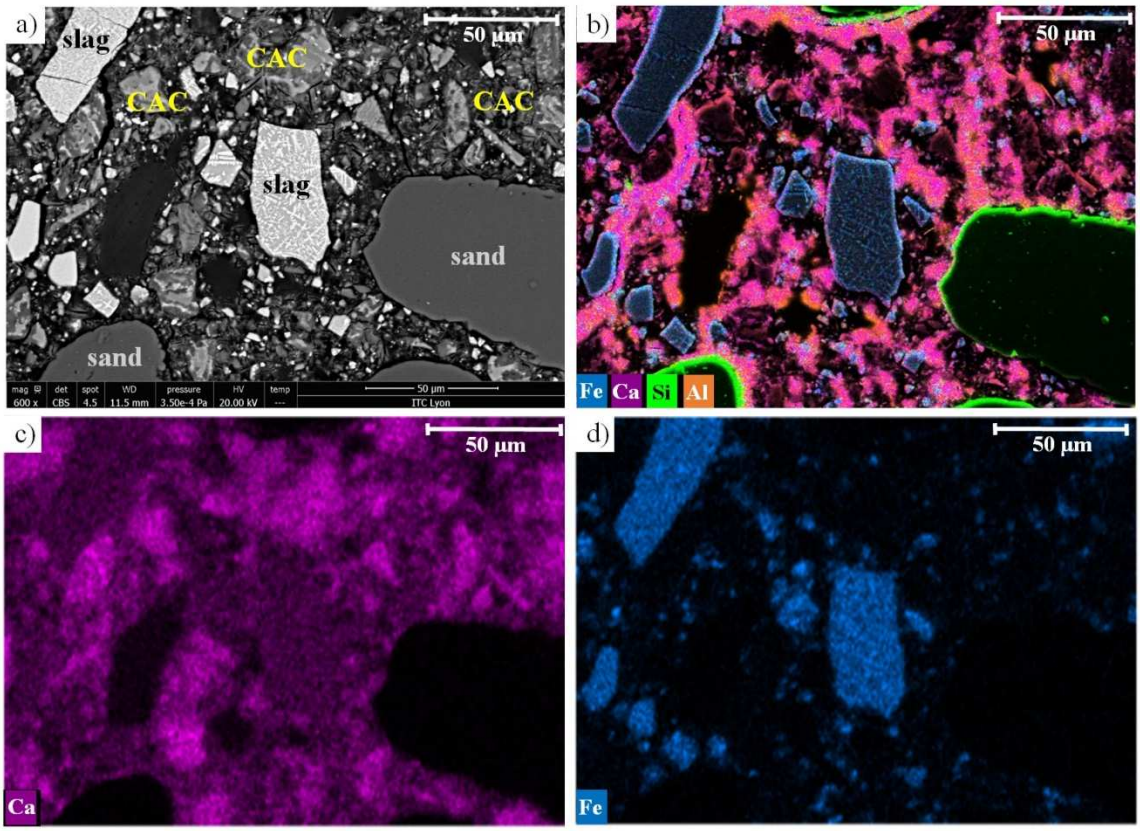

Figure 8 (a) SEM-BSE micrograph of slag-containing mortar sample after 90 days of hydration along with (b) the corresponding EDS mapping for Fe, Ca, Si, Al; (c) Ca alone and (d) Fe alone

Quantifying the degree of slag hydration could be possible following the dissolution of the slag calculated as the change in its total area between different curing ages. This method bears the assumption that the totality of the dissolved proportion of the slag is incorporated in the hydration products. Two critical challenges in applying this method to SEM micrographs include: (1) avoiding shadows in the images by obtaining an impeccably flat polished surface despite the highly contrasting abrasion resistance of the components of the paste samples and; (2) keeping the calculated degree of hydration representative despite the use of different samples per curing time when hydration is stopped. Considering these limitations, the degree of slag hydration using SEM-BSE combined with image analysis after 90 days of curing in paste samples (CAC-HH-slag formulation) was estimated at 15% [25]. To address the limitations encountered using this quantification technique, a nondestructive

test using XCT is performed combined with volume analysis based on grayscale gradient segmentation similar to the methodology demonstrated in a recent study by Wu et al. [24].

Figure 9 below presents the 3D volume render (a); a sample raw 2D reconstructed cross-section (b); a sample grayscale threshold segmentation to select the slag particles (c); and the corresponding 2D binary sections obtained after threshold segmentation of the hardened CAC-HH-slag paste formulations after 1, 28, 90, 180 and 365 continuous days of hydration. The particles shown in the 3D volume renders represent the undissolved (assumed as unreacted) slag particles shown as white areas in the binary images. The selection of the lower grayscale threshold limit for slag was guided by the plot profiles as demonstrated in **Figure 9** c where a distinct difference in the range of the grayscale index between slag and the other components of the hydrated paste in the raw reconstructed images can be clearly identified even prior to any image processing in CTAn. A maximum of ±5% deviation is introduced in the threshold segmentation to later assess the sensitivity of the calculated slag total volume percentage from which the slag reactivity values are derived. In addition to the plot profiles, the threshold segmentation was also guided by an earlier comparative analyses [25] using SEM-EDS micrographs described in the Methodology section. Although it was attempted to follow the same particles in the VOI per sample, it is important to note that the dimensional changes during the hydration and any small displacement during sample mounting in the holder are among the uncontrolled factors causing variations in the particles enclosed by the VOI between different curing periods. On the other hand, a representation of the previous XCT experiment [25] where hydration is stopped per sample and with a modified scan settings is presented in **Figure 10**. The 3D renders and the binary sections were recreated using CTVox and CTAn respectively to maintain a uniform representation as the results (**Figure 9**) obtained from the present methodology without stopping the hydration.

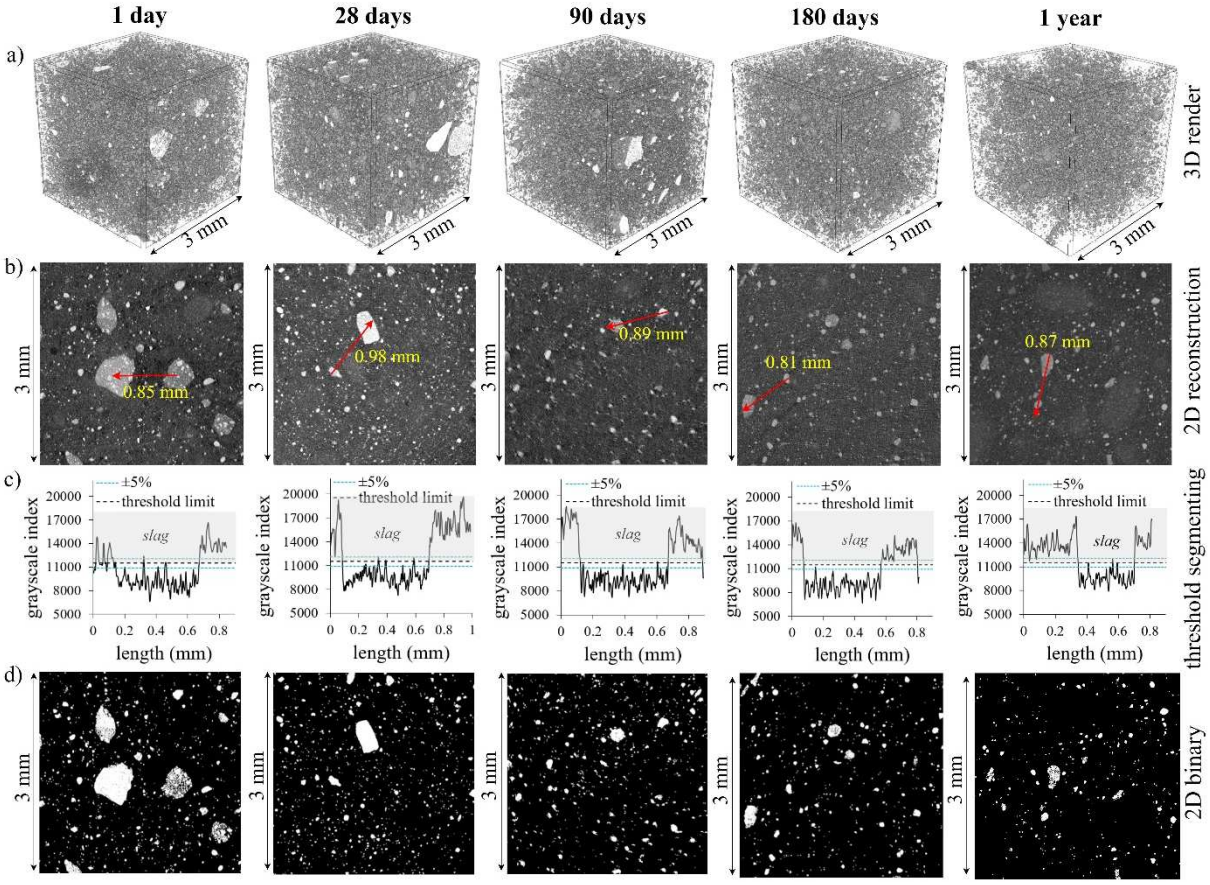

Figure 9 The (a) 3D volume render, (b) a sample raw 2D reconstructed cross-section, (c) grayscale threshold segmentation to select the slag particles, and (d) the corresponding 2D binary sections obtained from Nanotom X-ray computed tomography and image analysis (CTAn and Image J) of the hardened CAC-HH-slag paste formulations after 1, 28, 90, 80 and 365 continuous days of hydration. The length in c corresponds to the distance in the direction of the red arrows drawn in b.

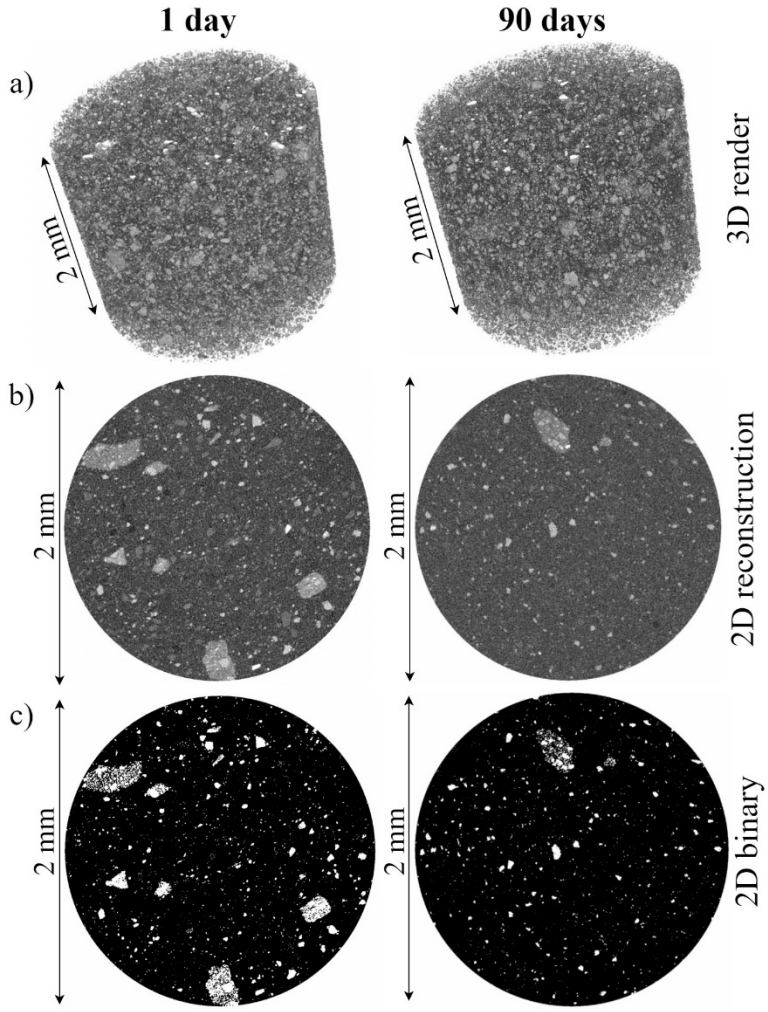

Figure 10 Representations of the (a) 3D volume render, (b) sample raw 2D reconstructed cross-section, and (c) their corresponding 2D binary sections obtained from Nanotom X-ray computed tomography and image analysis of the hardened CAC-HH-slag paste formulations after 1 and 90 days of curing followed by solvent exchange to stop the hydration [25]

The results of the quantification of the slag hydration degree are presented in **Figure 11** along with a sensitivity analysis demonstrating the effect of threshold segmentation to the calculated total volume percentage of slag. In **Figure 11** a, it can be observed that the calculated slag volume percentages vary proportionally across the sensitivity range. This could well imply that the calculated hydration degree values are relatively robust regardless of the variation in the grayscale threshold segmentation for the slag. The use of 16-bit reconstructed images during segmentation played an important role in minimizing the sensitivity as opposed to the standard 8-bit stack images (considering that CTAn is only capable of further custom processing of 8-bit images). Moreover, the results obtained from the

previous experiment [25] incorporating solvent exchange for stopping the hydration and using modified scan settings, although lower in absolute values, appear to have a relatively consistent trend with that of the current methodology. This could support the repeatability of the technique despite the changes in the sample preparation and the scan settings.

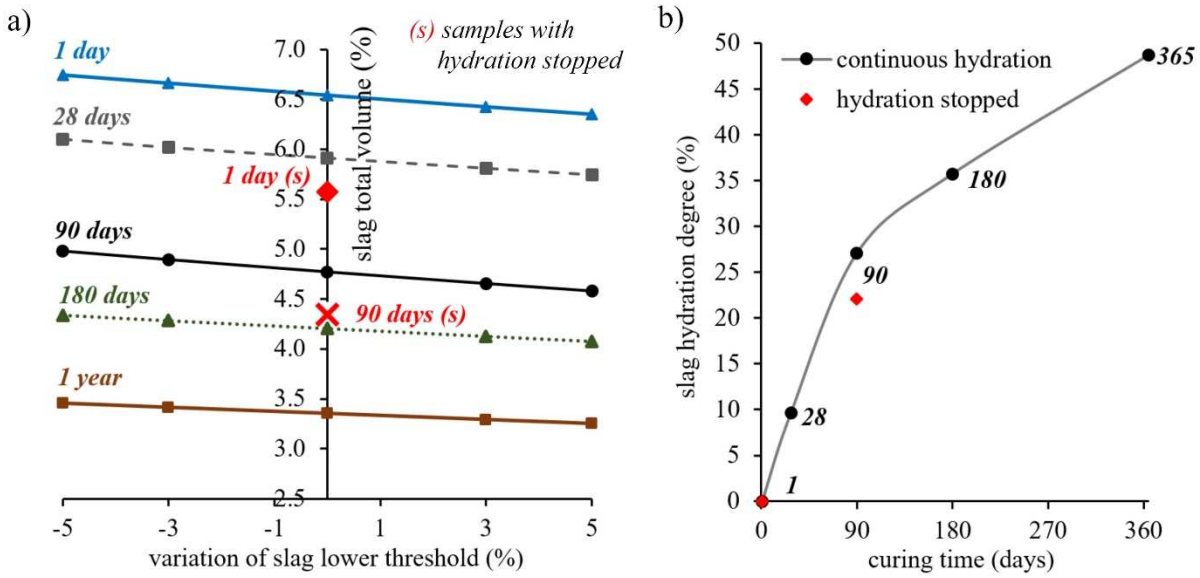

Figure 11 (a) Sensitivity analysis on the effect of the slag lower threshold limit segmentation to the values obtained for the total percent volume of the slag in the VOI; and (b) the corresponding degree of slag hydration at 28, 90, 180 and 365 days using 1 day as the base (zero slag hydration) reference. The samples where hydration is stopped prior to the scan are indicated by (s) and marked in red

The results in **Figure 11** b show that for the sample where hydration is continuous, only 9.6 % of the slag particles ≥ 2.15 µm (voxel resolution setting) is dissolved after 28 days of curing. This value progressively increased over time reaching up to 49% after 1 year. This is consistent with the trend of compressive strength (**Figure 3**) previously presented for the corresponding CAC-HH-slag mortar samples where it was concluded that the slag could have had a positive contribution to the long term hydration of the blend. Observing the slope in **Figure 11** b with no remarkable evidence of stagnation, it can be inferred that the slag dissolution will continue to progress beyond 1 year. It must be noted however that based on the particle size distribution (**Table 2**), about 20 wt.% of the slag falls below 2.15 µm representing the proportion of the slag particles not detectable by XCT due to the configuration of the voxel resolution. If it is speculated that the finest slag particles are the most

reactive given the higher surface area per weight exposed, this could mean that the calculated slag hydration degree values are greatly underestimated particularly in the early periods of curing which could also explain the drastic progression of the calculated hydration degree beyond 180 days. Conversely, increasing the resolution by decreasing the voxel size for instance would correspond to a longer scan time (not preferred due to active hydration) and/or smaller VOI requirement (less representative sample) to maintain the same skip size, exposure time and number of projections. Moreover, when compared to the value obtained (22 %) for the 90-day sample from the previous study [25] incorporating solvent exchange and modified scan settings (i.e. finer voxel resolution at 1.5 µm), the result from current methodology (at 27%) could still be considered to fall within an acceptable range.

In the end, selecting the appropriate methodology and scan settings is a matter of compensating among several factors to satisfy the objective of the study. For this case, the focus must be dedicated to the rate of the change in the slag hydration degree which can be compared more reliably using this technique rather than the absolute values. Accurately quantifying the hydration degree would require complementary technique/s (i.e. selective dissolution) if determining the absolute values of the reacted slag, as opposed to the relative reaction kinetics, is crucial. Compared to other hydration degree quantification techniques (i.e SEM-BSE + imaging, selective dissolution), XCT exemplifies the advantage of providing a rapid and accurate non-destructive alternative – taking only minutes for fast high resolution scans while eliminating rigorous sample preparations (i.e. stopping the hydration, polishing). Nonetheless, as this technique is still relatively new for such application, it is expected that further refining especially in selecting the parameters and operations in image analysis will be crucial in standardizing the methodology.

4 Conclusions

This study explores the properties of a CAC blended formulation incorporating an Fe-rich non-ferrous metallurgy slag as SCM. Compressive and flexural strength, setting time, dimensional stability, isothermal calorimetry, and the evolution of phase assemblage were followed through mortar and paste samples from 1 day to 1 year of curing. Additionally, a rapid non-destructive technique for

quantifying the degree of slag hydration is demonstrated using a combination of XCT and volume analysis.

Based on the results, the slag exhibited long term reactivity in the CAC-based formulation. However in the early age of hydration, the incorporation of the slag did not appear to contribute to the compressive strength nor have an apparent chemical effect on hydration. This is attributed to the slow dissolution of the slag only at about 10% (not accounting for the reactivity of the particles below 2.15 μm) after 28 days of curing based on the quantification using XCT coupled with volume analysis. It was not until after 28 days that the strength of the slag-containing mortars significantly increased with corresponding drastic improvement on the SAI values. At 90 days, the slag hydration degree was calculated to be at about 25% almost doubling up to 49% at 1 year indicating a significant slag dissolution and therefore could signify its influence on the properties of the blend.

In terms of the phase assemblage, ettringite quickly forms in the early hours of hydration contributing to the early strength of the blended systems with its expansive nature. As the sulfates are quickly consumed, ettringite decomposes into monosulfoaluminate. The late chemical reactions of the slag clearly altered the phase assemblage of the slag-containing formulation appearing to display an influence on the quantity of ettringite, AFm phases and hydrogarnet at longer curing period.

In the end, the observed properties of the slag (long term reactivity, strength development, setting time and dimensional stability) support the viability of its potential valorization as SCM in CAC blended systems. Given that the early strength property is critical in CAC applications, a forthcoming study has been dedicated towards unravelling the fate of Fe in the hydration as it comprises almost 50 wt.% of the slag. Elaborating a better understanding of the slag's hydration mechanism is used as a leverage to drive the development of activation techniques to increase its early age reactivity, therefore aiming to boost its potential for future valorization in this application.

5 Acknowledgements

J. Astoveza is grateful for receiving funding as an early-stage researcher of the SOCRATES Project under the European Union Framework Program for Research and Innovation Horizon 2020 Grant Agreement No.721385 (EU MSCA-ETN SOCRATES; project website: http://etn-socrates.eu). The

authors would also like to thank Dr. J. Soete from the Department of Materials Engineering of KU Leuven for his contributions in the previous work [25] involving the XCT which were referenced in this paper.

6 References

[1] R. Snellings, G. Mertens, J. Elsen, Supplementary Cementitious Materials, Rev. Min. Geochem. 74 (2012) 211–278.

[2] J. Astoveza, A. Abadias, R. Soth, R. Trauchessec, M. Reuter, Y. Pontikes, Industrial by-products as non-conventional supplementary cementitious material: YRSB19 - iiSBE Forum of Young Researchers in Sustainable Building, (2019).

[3] G.A. Blengini, F. Mathieux, L. Mancini, M. Nyberg, H.M. Viegas (Eds.), Recovery of critical and other raw materials from mining waste and landfills: State of play on existing practices, Publications Office of the European Union, Luxembourg, 2019.

[4] P.T. Jones, M. Lieven (Eds.), Proceedings of the 4th International Sympossium on Enhanced Landfill Mining, 2018.

[5] N. Saikia, G. Mertens, K. van Balen, J. Elsen, T. van Gerven, C. Vandecasteele, Pre-treatment of municipal solid waste incineration (MSWI) bottom ash for utilisation in cement mortar, J. Con. Build. Mat. 96 (2015) 76–85.

[6] Tang, P., Florea, M. V. A., Spiesz, P. R., & Brouwers, H. J. H (Ed.), The application of treated bottom ash in mortar as cement replacement, Istanbul, Turkey, 2014.

[7] J. Astoveza, R. Trauchessec, R. Soth, J. Salminen, Y. Pontikes, Assessing the reactivity of industrial by-products in calcium aluminate cement-based formulations, in: A. Malfliet, A. Peys, A. Di Maria (Eds.), Proceedings of the 6th International Slag Valorisation Symposium, 1-5 April 2019, Mechelen, Belgium: Science, innovation & entrepreneurship in pursuit of a sustainable world, KU Leuven, Materials Engineering, Leuven, 2019.

[8] N.M. Piatak, M.B. Parsons, R.R. Seal, Characteristics and environmental aspects of slag: A review, J. Ap. Geo. Chem. 57 (2015) 236–266.

[9] J.J. Emery (Ed.), Slag utilization in pavement construction: Extending aggregate resources ASTM STP, 1982.

[10] J.D. Bapat, Mineral admixtures in cement and concrete, CRC Press, Boca Raton, 2013.

[11] S.C. Pal, A. Mukherjee, S.R. Pathak, Investigation of hydraulic activity of ground granulated blast furnace slag in concrete, Cement and Concrete Research 33 (2003) 1481–1486.

[12] Y. Feng, J. Kero, Q. Yang, Q. Chen, F. Engström, C. Samuelsson, C. Qi, Mechanical Activation of Granulated Copper Slag and Its Influence on Hydration Heat and Compressive Strength of Blended Cement, Materials (Basel, Switzerland) 12 (2019).

[13] P.N. Benkendorff, Potential of lead/zinc slag for use in cemented mine backfill, Mineral Processing and Extractive Metallurgy 115 (2013) 171–173.

[14] V. Hallet, N. de Belie, Y. Pontikes, The impact of slag fineness on the reactivity of blended cements with high-volume non-ferrous metallurgy slag, Construction and Building Materials 257 (2020) 119400.

[15] K. Murari, R. Siddique, K.K. Jain, Use of waste copper slag, a sustainable material, J Mater Cycles Waste Manag 17 (2015) 13–26.

[16] I. Alp, H. Deveci, H. Süngün, Utilization of flotation wastes of copper slag as raw material in cement production, J. Haz. Mat. 159 (2008) 390–395.

[17] M. Penpolcharoen, Utilization of secondary lead slag as construction material, Cem. Con. Res. 35 (2005) 1050–1055.

[18] S.H.G. Mosavinezhad, S.E. Nabavi, Effect of 30% Ground Granulated Blast Furnace, Lead and Zinc Slags as sand replacements on the strength of concrete, KSCE J. Civ. Eng. 16 (2012) 989–993.

[19] M. Alwaeli, Application of granulated lead–zinc slag in concrete as an opportunity to save natural resources, J. Rad. Phys. Chem. 83 (2013) 54–60.

[20] M.A. Chavda, H. Kinoshita, J.L. Provis, Modification of a calcium aluminate cement system to prevent conversion to cubic hydrates and minimise corrosion of encapsulated aluminium metal: 32nd Cement and Concrete Science Conference, Queen's University Belfast, 17-18 September.

[21] J. Bizzozero, Hydration and dimensional stability of calcium aluminate cement based systems. Dissertation, Lausanne, Switzerland, 2014.

[22] H. Nguyen, P. Kinnunen, K. Gijbels, V. Carvelli, H. Sreenivasan, A.M. Kantola, V.-V. Telkki, W. Schroeyers, M. Illikainen, Ettringite-based binder from ladle slag and gypsum – The effect of citric acid on fresh and hardened state properties, Cement and Concrete Research 123 (2019) 105800.

[23] M.U. Okoronkwo, F.P. Glasser, Stability of strätlingite in the CASH system, Mater Struct 49 (2016) 4305–4318.

[24] Z. Wu, Y. Wei, S. Wang, J. Chen, Application of X-Ray Micro-CT for Quantifying Degree of Hydration of Slag-Blended Cement Paste, J. Mater. Civ. Eng. 32 (2020) 4020008.

[25] J. Astoveza, J. Soete, R. Trauchessec, R. Soth, Residual matrix valorisation as supplementary cementitious materials in calcium aluminate blended cements: Quantification of the Degree of Slag Hydration by Image Analysis (oral presentation), International Process Metallurgy Symposium, Espoo, Finland, 2019.

[26] A.A. Ramezanianpour, Cement Replacement Materials: Properties, Durability, Sustainability, Springer, Berlin, Heidelberg, 2014.

[27] M. Juenger, M. Won, D. Fowler, C. Suh, A. Edson, Effects of Supplementary Cementing Materials on the Setting Time and Early Strength of Concrete: Technical Report FHWA/TX-08/0-5550-1, 2007, https://ctr.utexas.edu/wp-content/uploads/pubs/0_5550_1.pdf.

[28] K. Scrivener (Ed.), Advanced Concrete Technology: Chapter: Calcium Aluminate Cements, Elsevier, 2003.

[29] W. Nocuń-Wczelik, Z. Konik, A. Stok, Blended systems with calcium aluminate and calcium sulphate expansive additives, Construction and Building Materials 25 (2011) 939–943.

[30] C. Cau Dit Coumes, S. Courtois, S. Peysson, J. Ambroise, J. Pera, Calcium sulfoaluminate cement blended with OPC: A potential binder to encapsulate low-level radioactive slurries of complex chemistry, Cement and Concrete Research 39 (2009) 740–747.

[31] S. Berger, C. Cau Dit Coumes, P. Le Bescop, D. Damidot, Stabilization of ZnCl2-containing wastes using calcium sulfoaluminate cement: cement hydration, strength development and volume stability, Journal of hazardous materials 194 (2011) 256–267.

[32] P. Feng, C. Miao, J.W. Bullard, Factors influencing the stability of AFm and AFt in the Ca-Al-S-O-H system at 25 °C, Journal of the American Ceramic Society 99 (2016) 1031–1041.

[33] D. Damidot, B. Lothenbach, D. Herfort, F.P. Glasser, Thermodynamics and cement science, Cement and Concrete Research 41 (2011) 679–695.

[34] Y. Xi, D.D. Siemer, B.E. Scheetz, Strength development, hydration reaction and pore structure of autoclaved slag cement with added silica fume, Cement and Concrete Research 27 (1997) 75–82.

[35] N.Y. Mostafa, Z.I. Zaki, O.H. Abd Elkader, Chemical activation of calcium aluminate cement composites cured at elevated temperature, Cement and Concrete Composites 34 (2012) 1187–1193.

[36] H.G. Midgley, Quantitative determination of phases in high alumina cement clinkers by X-ray diffraction, Cement and Concrete Research 6 (1976) 217–223.

[37] F. Wang, P. Chen, X. Li, B. Zhu, Effect of Colloidal Silica on the Hydration Behavior of Calcium Aluminate Cement, Materials (Basel, Switzerland) 11 (2018).

[38] A.A. Hilal, Microstructure of Concrete, in: S. Yilmaz, H.B. Ozmen (Eds.), High Performance Concrete Technology and Applications, InTech, 2016.

[39] H.G. Midgley, P. Bhaskara Rao, Formation of stratlingite, 2CaO.SiO2.Al2O3.8H2O, in relation to the hydration of high alumina cement, Cement and Concrete Research 8 (1978) 169–172.

[40] Z. Xiaowei, L. Chunxia, S. Junyi, Influence of tartaric acid on early hydration and mortar performance of Portland cement-calcium aluminate cement-anhydrite binder, Construction and Building Materials 112 (2016) 877–884.

[41] D. Torréns-Martín, L. Fernández-Carrasco, M.T. Blanco-Varela, Conduction calorimetric studies of ternary binders based on Portland cement, calcium aluminate cement and calcium sulphate, J Therm Anal Calorim 114 (2013) 799–807.

[42] A. Fernández-Jiménez, T. Vázquez, A. Palomo, Effect of Sodium Silicate on Calcium Aluminate Cement Hydration in Highly Alkaline Media: A Microstructural Characterization, Journal of the American Ceramic Society 94 (2011) 1297–1303.

[43] A. Malfliet, A. Peys, A. Di Maria (Eds.), Proceedings of the 6th International Slag Valorisation Symposium, 1-5 April 2019, Mechelen, Belgium: Science, innovation & entrepreneurship in pursuit of a sustainable world, KU Leuven, Materials Engineering, Leuven, 2019.

[44] G. Möschner, B. Lothenbach, F. Winnefeld, A. Ulrich, R. Figi, R. Kretzschmar, Solid solution between Al-ettringite and Fe-ettringite (Ca6[Al1−xFex(OH)6]2(SO4)3·26H2O), Cement and Concrete Research 39 (2009) 482–489.

[45] B.Z. Dilnesa, B. Lothenbach, G. Renaudin, A. Wichser, D. Kulik, Synthesis and characterization of hydrogarnet Ca3(AlxFe1−x)2(SiO4)y(OH)4(3−y), Cement and Concrete Research 59 (2014) 96–111.

[46] B.Z. Dilnesa, E. Wieland, B. Lothenbach, R. Dähn, K.L. Scrivener, Fe-containing phases in hydrated cements, Cement and Concrete Research 58 (2014) 45–55.